Journal of
Synchrotron Radiation

ISSN 0909-0495

Received 23 December 2011
Accepted 5 April 2012

Coalescence analysis for evolving foams *via* optical flow computation on projection image sequences

Anton Myagotin,[a]* Alexey Ershov,[b] Lukas Helfen,[b] Raquel Verdejo,[c] Alexander Belyaev[d] and Tilo Baumbach[b]

[a]Saint Petersburg State University of Civil Aviation, Pilotov 38, 196210 Saint Petersburg, Russia, [b]ANKA – Institute for Synchrotron Radiation, Karlsruhe Institute of Technology, D-76021 Karlsruhe, Germany, [c]Institute of Polymer Science and Technology, (ICTP-CSIC), Juan de la Cierva 3, 28006 Madrid, Spain, and [d]Institute for Problems in Mechanical Engineering (RAS), VO Bolshoj pr. 61, 199178 Saint Petersburg, Russia. E-mail: anton.myagotin@gmail.com

A novel image-processing procedure is proposed for the analysis of sequences of two-dimensional projection images. Sudden events like the merging of bubbles in an evolving foam can be detected and spatio-temporally located in a given projection image sequence. The procedure is based on optical flow computations extended by a forward–backward check for each time step. Compared with prior methods, efficient suppression of noise or false events is achieved owing to uniform foam motion, and the reliability of detection is thus increased. The applicability of the proposed procedure in combination with synchrotron radiography is illustrated by a series of characteristic studies of foams of different kind. First, the detection of single-bubble collapses in aqueous foams is considered. Second, a spatial distribution of coalescence events in metals foamed in casting molds is estimated. Finally, the structural stability of polymer foams containing admixed solid nanoparticles is examined.

Keywords: radiography; foam; image analysis; optical flow.

1. Introduction

The production, characterization and application of foams and sponges has attracted increasing attention over the last decade (Schüth *et al.*, 2002). Foams and sponges exhibit remarkable properties, for example large surface-to-volume ratios or the combination of low weight with high mechanical stiffness. Such porous materials are therefore beneficial and thus widely employed in a broad range of industrial, medical and scientific applications.

The formation and decay of foams, *i.e.* 'foaming', is a complex interplay of physical phenomena such as drainage, coalescence, coarsening, topological transformations, pore inflation, *etc.* (Weaire & Hutzler, 1999). Although some foams, for example metal foams produced by the powder-metallurgical method, start their early expansion already in the solid state (Stanzick *et al.*, 2002; Helfen *et al.*, 2003), the final structure of a generated foam results from the temporal evolution, stability and ageing of a dispersion gas–liquid system.

Suitable tools are required for monitoring and characterizing the foaming process, *i.e.* its dynamical behaviour. An important dynamical effect during foaming is coalescence, *i.e.* the process of merging two (or more) bubbles into a single one by the rupture of separating liquid films acting as bubble walls. It is widely believed that the physical reason for film rupture is the instability of liquid films owing to increased surface tension (Carrier & Colin, 2003). Because of an excess of capillarity pressure and gas diffusion the foam films are stretching and thinning out. The surface tension increases and, after attaining a certain critical thickness, leads to film rupture and pore coalescence. Theoretical models of drainage and coalescence can be found in the literature (Bhakta & Ruckenstein, 1997; Gergely & Clyne, 2004; Ireland, 2009). However, the correspondence of these models with real foaming processes is still far from being completely established.

Compared with the coarsening process due to gas diffusion between neighbouring bubbles, coalescence is rather fast and therefore requires higher temporal resolution for appropriate investigation. For different kinds of foams a variety of experimental tools and methods have been developed to gain insight into the foam dynamics.

Since foams are heterogeneous materials being non-stable in time and owing to the spontaneous nature of rupture events, detecting and quantifying coalescence in a reliable manner is not a trivial task. A liquid-film rupture in real foams is usually of short duration, *e.g.* ∼2 ms in aqueous (Vandewalle *et al.*, 2001) and about 600 µs in metal foams (García-Moreno *et al.*, 2008), compared with other processes modifying the foam structure [except for topological transitions which occur sometimes on the same time scale, *e.g.* T1 transitions (Biance

et al., 2009) induced under shear strain]. Indirect studies of coalescence in foams have been performed, for example, using conductivity profiles (Dale *et al.*, 1999), acoustic measurements (Müller & di Meglio, 1999), and neutron (Belaroui *et al.*, 2003) and visible-light scattering (Søndergaard & Lyngaae-Jørgensen, 1996). Bubble collapses in transparent aqueous foams can also be registered by the use of an optical camera working at a high frame rate (Rouyer *et al.*, 2003).

X-ray imaging is particularly adapted to the study of opaque materials (Banhart *et al.*, 2001*a*). The short wavelength and reduced interaction of X-rays with matter (compared with other spectral ranges) often allows one to describe image formation by a propagation along straight lines. Therefore, X-rays are also suitable for foams which would strongly scatter other probing radiation. The combination with computed tomography provides a powerful tool for obtaining three-dimensional (3D) information on the structural evolution. The method has been successfully applied to foams for *ex situ* analysis focusing on the morphological and physical properties (Maire & Buffiere, 2000; Helfen *et al.*, 2002, 2005; Rack *et al.*, 2009*b*).

The high brilliance and high flux density of synchrotron radiation has been exploited for *in situ* tomography studies. Tomography has the disadvantage that many projection images are required to reconstruct the 3D structure under observation. Compared with radiographic imaging, this inherently reduces the temporal resolution that can be attained. Such *in situ* 3D measurements could therefore be carried out only in the case of rather stable foams, *i.e.* where the microstructural changes occur on a time scale that is longer than the duration of a single tomography scan. Nevertheless, the slower dynamical effects related to gas generation (Babin *et al.*, 2006) or diffusion (Lambert *et al.*, 2007, 2010) could effectively be visualized.

Abandoning the concept of 3D imaging and restricting the measurements to fast recording of projected radiographic sequences, the evolution of porous structure can be observed with a high temporal resolution. In particular, the high X-ray flux density in *in situ* synchrotron radiography (Banhart *et al.*, 2001*a*) allows for fast image acquisition rates with a low noise level. Recent studies show that synchrotron radiation is applicable for the generation of projection radiographs and, consequently, for the investigation of foam dynamics of different types, *e.g.* metal (Banhart *et al.*, 2001*b*) or polymeric (Verdejo *et al.*, 2009) foams.

Along with the high flux density, modern detector technology has enabled synchrotron radiation radiography to investigate dynamical properties of foaming processes with exposure times down to the microsecond level which allows rates of several thousands of frames per second (García-Moreno *et al.*, 2008; Rack *et al.*, 2009*a*). This example shows that, even with short experimental durations of the order of seconds, several tens of thousands of radiographs can be acquired and need to be evaluated. For this reason, an automated analysis procedure for image sequences would be of enormous assistance in investigating the data acquired.

In this paper we suggest a novel image-processing procedure which increases the reliability of the localization of coalescence events in evolving foams *via* projection imaging. The peculiarity of the radiographic method is that the sample structure is projected onto a two-dimensional image plane at the detector. This implies that the depth information is irretrievably lost in the direction of the X-ray beam. In projection images, foaming appears as a rapidly changing complex arrangement of overlapping pores, bubbles and foam films. This explains why early investigations of coalescence processes in radiographic series have been mainly restricted to the counting of individual film ruptures by a human observer (*e.g.* Wübben *et al.*, 2003), which is clearly a tedious and erroneous task. This paper addresses the problem of an automated and reliable quantification of coalescence processes in radiographic series. In comparison with our former approach (Myagotin *et al.*, 2009), here we employ a more general formalism, *i.e.* a method based on optical flow computations. The latter is a well known problem statement in computer vision. We show that the identification of disrupt motion patterns in a time-ordered radiographic image series provides a viable solution to the problem of coalescence detection.

This work overviews the challenges appearing during the analysis of projection radiographs, gives a survey and classification of existing image-processing methods, and compares their advantages and drawbacks. The article is organized as follows. §2 describes a standard set-up for the generation of projection images and enumerates experimental conditions to be fulfilled to produce viable estimations. §3 shows how a coalescence study can be reduced to optical flow computations with the subsequent flow analysis. Using signal detection theory we evaluate the accuracy of the developed image-processing routine in §4. We discuss the applications of the novel approach to foams of different types in §5. The possibility for the detection of individual bubble collapses is shown by an example of aqueous foams. Further, we estimate coalescence distribution maps for metal foams generated in steel molds. Finally, we examine the temporal structure stability of polymer foams filled with nanoparticles.

2. Experimental set-up

A typical radiographic experiment includes a radiation source illuminating an investigated sample, mechanical manipulators for placing the sample in the beam path, and a two-dimensional detector system. Among the real-time detectors one distinguishes systems of direct photon counting, where photons are directly converted into electrical charge distributions, and systems with indirect photon detection, in which the X-ray beam is converted into visible light and further registered by a light-sensitive two-dimensional area detector, *e.g.* based on a charge-coupled device (CCD) (Gruner *et al.*, 2002). Digital radiographic images are recorded by readout electronics with a temporal sampling period and transferred to a general-purpose computer system for further processing.

A proper choice of the sampling period τ is important. For a temporally band-limited process characterized by a Nyquist rate r_N, we call the process 'continuous' if the relation $r_N \leq 1/(2\tau)$ is fulfilled. Having a series of radiographs recorded at discrete time intervals enables us to trace the underlying changes during a process in a lossless way. Conversely, if the above relation does not hold, the process under consideration is declared to be 'discontinuous'. Consequently, a coalescence event detection becomes possible if τ is set to follow foam structure modifications, except much faster film ruptures. Thus, the coalescence process can be unambiguously attributed to the discontinuous part of foaming, whereas all other effects belong to continuous processes fulfilling the sampling condition. It is worth mentioning that if the duration of coalescence events is of the same order of magnitude as the characteristic duration of other dynamical effects, it is not possible to define a proper sampling period allowing for clear distinguishing between them.

In order to permit the estimation of the characteristics from radiographic images, a couple of general assumptions should be explained. We assume that coalescence events are randomly distributed over the sample interior. Moreover, the process under consideration has to be statistically isotropic, *i.e.* the statistical properties of the sample observed from any particular direction are identical. Finally, the thickness of the sample should be chosen in such a way that the contrast of radiographic images is high enough to observe foam constituents.

3. Optical flow analysis

In a time-ordered series of digital images a principle difference between continuous and discontinuous features is that the former are trackable from one frame to another. For an image sequence $f(x, y, t)$, where (x, y) are the coordinates within an image domain, this property is formally expressed by a brightness constancy assumption (Horn & Schunck, 1981),

$$f\big(x + \delta_x, y + \delta_y, t + \tau\big) \simeq f(x, y, t), \tag{1}$$

stating that a pixel at time $t + \tau$ is the original pixel at time t displaced by an offset (δ_x, δ_y). Applying the Taylor expansion to the brightness function,

$$\begin{aligned} f(x + \delta_x, y + \delta_y, t + \tau) = f(x, y, t) \\ + \frac{\partial}{\partial x} f\,\delta_x + \frac{\partial}{\partial y} f\,\delta_y + \frac{\partial}{\partial t} f\,\tau \\ + o(\delta_x^2, \delta_y^2, \tau^2), \end{aligned} \tag{2}$$

one derives a so-called optical flow equation

$$-f_t = \nabla f \cdot \mathbf{u}^T, \tag{3}$$

where $\mathbf{u} = (\delta_x/\tau, \delta_y/\tau)$ is a velocity vector and $\nabla f = (f_x, f_y)$ is a spatial brightness gradient. Computations of the vector field $\mathbf{u}$ from two successive images is termed an 'optical flow' problem (Horn & Schunck, 1981).

The presence of motion discontinuities violates the brightness constancy assumption leading to a degraded accuracy of optical flow computations. Therefore they are usually treated by conventional image-processing methods as an unwished side effect, an artefact that should be eliminated or at least suppressed. Although there are a number of algorithms dealing with temporal or spatial discontinuities in optical flow (*e.g.* Middendorf & Nagel, 2001; Alvarez *et al.*, 2007), methods employing the detection or evaluation of discontinuous features themselves have not been derived so far.

The discontinuities in optical flow for a given process can be boosted by intentionally introduced temporal undersampling. Moreover, they correspond to real physical phenomena, namely to the bubble collapses and film ruptures. A naive approach for the event detection utilizes a slow motion assumption, *i.e.* the offset (δ_x, δ_y) for all image pairs is assumed to be small. Thus, a high difference between the successive frames, which is greater than a predefined threshold,

$$|f(x, y, t + \tau) - f(x, y, t)| > T_\varepsilon, \tag{4}$$

indicates for the position (x, y) an occurrence of a coalescence event. The naive approach itself fails to distinguish between complex foam motion accompanied by geometrical distortions and film destructions, *i.e.* it is restricted to almost static foams.

The basic detection model can be extended by applying a set of morphological operators on the difference image to filter structures of a certain size. A similar approach was discussed earlier by García-Moreno *et al.* (2003): various image-processing filters have been applied to a given sequence of difference images in order to improve the detection of liquid film ruptures. As a result, the amount of mistakenly detected events is reduced. However, this approach discriminates between different sizes of the detected events and is still prone to fail in the presence of fast movements.

The concept of a static foam can be replaced by a more realistic assumption of linear motion. Within a small image region the movement of foam constituents is viewed as a linear displacement. The computed vector field $\mathbf{u}$ is used to perform a motion-compensated difference. In this method the difference between the original first frame and the motion-compensated second frame,

$$|f(x + \delta_x, y + \delta_y, t + \tau) - f(x, y, t)| > T_\varepsilon, \tag{5}$$

indicates motion-aware temporal changes at the image location (x, y). For the motion computation it is common to choose correlation-based methods (Dzieciol *et al.*, 2009; Dubsky *et al.*, 2010). In such methods a displacement field is computed by maximizing the product (or cross correlation) of aligned images,

$$\sum_{x,y} f(x + \delta_x, y + \delta_y, t + \tau) f(x, y, t) \;\rightarrow\; \max. \tag{6}$$

Although the implementation of such techniques is straightforward, the simple correlation approach shows only average performance. In order to deal with rotational motion, large displacements and non-uniqueness of the solution in homogeneous image areas, more sophisticated modifications of the correlation method are required.

An alternative approach for coping with large displacements is based on Fourier analysis. According to the Fourier shift theorem the image regions corresponding to moving features have identical amplitude spectra. Thus, a high difference

$$|\mathcal{FT}\{f_{t+\tau}\}| - |\mathcal{FT}\{f_t\}| > T_\varepsilon \tag{7}$$

is evidence of the presence of a coalescence event. This approach was examined earlier by Myagotin *et al.* (2009). By subdividing two successive images into small partitions, one excludes sequentially the regions containing local shifts only. The major drawback of the method is that non-linear distortions are not taken into account (which are highly probable owing to expansion and deformation of pores). This leads to erroneous attribution of these image regions to coalescence events.

Recent achievements in the field of optical flow computations allow one to estimate a vector field $\mathbf{u}$ in an image sequence with high accuracy and in real time, even in the presence of motion discontinuities and noise (Bruhn & Weickert, 2005; Zimmer *et al.*, 2011; Baker *et al.*, 2011). In this work we propose an extension of the variational optical flow methods, called a forward–backward check, for the construction of an improved coalescence event detector: applying the optical flow method the distributions of velocity vectors for an original radiographic sequence and for the sequence with the reversed order of frames are computed. The estimates are referred to as forward $\mathbf{u}^{\mathrm{f}}$ and backward $\mathbf{u}^{\mathrm{b}}$ vectors. For trackable image features the vector fields should be consistent such that the relation

$$||\mathbf{u}^{\mathrm{f}} + \mathbf{u}^{\mathrm{b}}|| \rightarrow \min \tag{8}$$

holds, as is shown in Fig. 1(*a*). *Vice versa*, a high magnitude of the discrepancy vector

$$||\Delta\mathbf{u}|| = ||\mathbf{u}^{\mathrm{f}} + \mathbf{u}^{\mathrm{b}}|| > T_\varepsilon \tag{9}$$

can be used as an indicator revealing discontinuities between two frames. In our approach no reduction in the imaging resolution nor a binarization intrinsically occurs as in the approach described by Myagotin *et al.* (2009).

For the velocity field computations we apply a variational optical flow method initially described by Brox *et al.* (2004). The incorporated optical flow model employs the brightness constancy assumption and a flow-driven smoothness term. The solution of the optical flow equation (3) is found as a minimizer of the energy functional

$$E(\delta_x, \delta_y) = \int_{\Omega_2} \left[f(x+\delta_x, y+\delta_y, t+\tau) - f(x,y,t) \right]^2 + S(\delta_x, \delta_y)\,\mathrm{d}x\,\mathrm{d}y. \tag{10}$$

The flow-driven smoothness term S is of the form

$$S(\delta_x, \delta_y) = \alpha\Psi\left[\left(\frac{\partial\delta_x}{\partial x}\right)^2 + \left(\frac{\partial\delta_x}{\partial y}\right)^2 + \left(\frac{\partial\delta_y}{\partial x}\right)^2 + \left(\frac{\partial\delta_y}{\partial y}\right)^2 \right], \tag{11}$$

where $\alpha \in R^+$ is a smoothness parameter and Ψ is a quadratic penalizer function,

$$\Psi(s) = (s+\varepsilon)^{1/2}, \tag{12}$$

with a small constant ε introduced for numerical reasons in order to avoid an unbounded denominator after differentiation.

The flow-driven smoothness constraint allows for discontinuities in the motion field and provides reliable flow estimation even in homogeneous image regions. In order to solve for large displacements a multi-scale computation scheme is employed. For more details on the implementation, the reader is referred to the original paper. For the data constancy assumption in variational model (10) we intentionally choose a non-robust setting over a robust one to magnify the influence of discontinuities (*e.g.* bubble collapses) on the motion estimation model. This significantly improves the performance of the forward–backward check method.

The advantages of the proposed variational optical flow model are a high accuracy, robustness against noise and the possibility to select an appropriate model for the given imaging conditions and motion types. However, the flexibility of the method is associated with an increased number of intrinsic parameters for the motion estimation and an additional implementation effort. Nevertheless, we are confident that the advantages and improvements over traditionally employed methods clearly outweigh the additional effort.

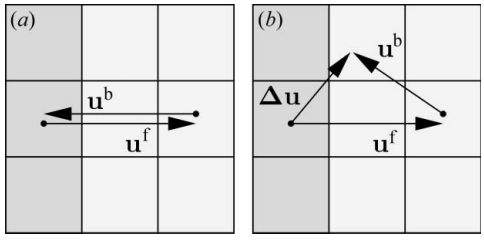

Figure 1
Forward–backward check: (*a*) consistent vector field; (*b*) deviation between the forward and backward velocity vectors occurs owing to a discontinuous feature.

4. Performance analysis

From the viewpoint of signal detection theory, a coalescence registration method can be considered (in a simplification) as a binary classifier, deciding for each pixel of an input image whether or not it belongs to the projection of a coalescence event. A common way to evaluate the accuracy for a given classifier is to count so-called 'hits' and 'false alarm' events (Wickens, 2001). Adopting this approach, we define the true positive rate (TPR) as

$$\mathrm{TPR} = N_{\mathrm{TP}}/S_{\mathrm{T}}, \tag{13}$$

that is the number N_{TP} of pixels correctly attributed to coalescence normalized to the event projection area S_{T}, and the false positive rate (FPR) as

$$\mathrm{FPR} = N_{\mathrm{FP}}/S_{\mathrm{F}}, \tag{14}$$

that is the normalized number N_{FP} of pixels mistakenly marked as an event. It should be noted that the sum of areas S_T and S_F gives the total area of an input image.

Since it is not possible to determine unambiguously the ground truth (*e.g.* film rupture) in real radiographs, our performance analysis is based on a simple simulation model of foaming where motion and structural expansion are accompanied by coalescence. We put a 3D tomographic image of a metal foam sample acquired by high-resolution computed tomography in a virtual laboratory. The dataset was shifted with a constant velocity and elastic deformation was performed to model foam expansion. A coalescence event is modelled by setting the material density to zero within a spherical region of a randomly selected size and location. From the set of 3D volumes describing the temporal evolution of the foam, a series of projection images is generated by a ray-tracing technique. Although the described model does not simulate real physical aspects of foaming properly, it incorporates the disappearance of foam constituents combined with non-uniform motion and growth, which are sufficient conditions to test coalescence detectors.

The evaluation results for the described image-processing methods are summarized in Fig. 2. The curves represent the receiver operation characteristic (ROC) of a given method, which maps the false positive and true positive rates for different thresholds (Metz, 1978; Swets *et al.*, 2000). Each curve has two common points: point (0, 0) corresponds to the case when a threshold is set too high and neither hits nor false alarms are registered. The point (1, 1) identifies that there is a low threshold so that an entire image is recognized as an event. The dashed line connecting both points denotes the ROC curve of the worst possible detector which produces a decision by a uniformly distributed guess.

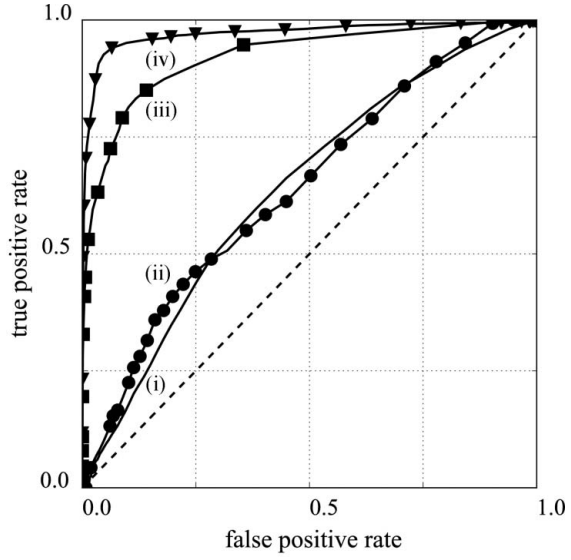

Figure 2
ROC curves measured from simulated data for the simple difference approach (i), the difference approach extended with morphological operations (ii), the Fourier shift detection approach (iii) and variational optical flow with the forward–backward check (iv).

In the comparison study we included four coalescence detectors: (i) a simple difference approach, (ii) difference extended by morphological erosion and dilation (used to filter out motion-related artifacts), (iii) Fourier shift detection method described by Myagotin *et al.* (2009), and (iv) our novel variational optical flow approach combined with a forward–backward check. The measured characteristics clearly highlight an inability of both difference-based approaches to provide a high detection quality for non-static structures. The area under a curve (AUC), which can be used as a single-valued measure of accuracy, does not attain 0.7 while an acceptable value for a binary classifier is 0.75 and higher (Swets, 1988). On the contrary, the Fourier shift detection is more reliable even for sequences with non-linear distortions. Its estimated AUC value is close to 0.93. Owing to a high accuracy of vector field computations by variational optical flow, the developed method possesses an extraordinary characteristic (iv), which is close to an ideal detector. In all conducted tests, measured AUC values varied in the range 0.97–0.98 suggesting the method to be a proper choice for practical applications.

Although the method has proven to perform well on synthetic sequences, one has to point out a principle case limiting its immediate widespread application. The image processing is based on the assumption that the duration of a coalescence event significantly differs from that of other dynamical effects. The discontinuities detected in this case are correctly attributed to coalescence. If the above condition is not fulfilled, however, all other fast processes occurring on the same time scale, such as sudden topological transitions T1 (Durand & Stone, 2006), will be detected as well. These T1 topological transitions are predominantly for a certain range of foams [*e.g.* strained stable aqueous foams (Biance *et al.*, 2009)] and can be neglected for others (*e.g.* rather unstable metal foams). The presence and relative frequency has therefore to be determined beforehand in order to exclude biased detection results. Moreover, the forward–backward check could also be extended by a more sophisticated post-processing procedure (*e.g.* employing morphological operations) to filter out discontinuities corresponding exclusively to coalescence.

5. Applications

This section demonstrates a number of applications where optical flow computations combined with the forward–backward check can be used as an analysis tool in order to perform coalescence studies and to assess the stability of evolving foams. In particular, we consider aqueous, metal and polymer foam samples monitored by X-ray radiography. The corresponding experiments were conducted at the ID19 beamline (Weitkamp *et al.*, 2010) of the European Synchrotron Radiation Facility (ESRF) in Grenoble, France. The essential information concerning experimental conditions is summarized in Table 1.

Table 1
Experimental conditions chosen for the imaging experiments conducted at beamline ID19 (Weitkamp *et al.*, 2010) of the ESRF.

Name	Sample	X-ray energy	Detector pixel size	Image frequency	Remarks
Aqueous foam (§5.1)	Aqueous solution with 0.1% dishwasher liquid	17.7 keV	1.75 µm	3 Hz	Foaming in a test tube at room temperature
Metal foam (§5.2)	AlSi7 powder admixed with TiH_2 (0.5 wt%)	33 keV	40 µm	2 Hz	Foaming in a steel mold, and furnace at $T \simeq 998$ K
Polymer foam (§5.3)	Polydimethylsiloxane (PDMS)	20 keV	2.8 µm	10 Hz	Foaming in a test tube at room temperature

5.1. Aqueous foams

The straightforward application for the optical flow analysis is an automatic detection and registration of individual pore collapses. In our first experiment we generated a long radiographic sequence consisting of 500 frames and depicting the evolution of aqueous foam. Owing to a high stability of the sample only a few collapses are present there. We present here two common cases of bubble rearrangements. Examining the original radiographs of Figs. 3(*a*), 3(*b*), 3(*f*) and 3(*g*) one understands that a manual search to find the few events through the entire sequence is clearly a time-consuming task. The top row (*a*)–(*e*) corresponds to the case where displacements of foam constituents are present exclusively (*e.g.* owing to a coalescence event outside the field of view). The images in the bottom row (*f*)–(*j*) show the collapse of a bubble combined with the motion (displacement) of surrounding foam constituents between the two successive frames (*f*, *g*). A comparison of all techniques discussed so far is shown in Figs. 3(*c*)–(*e*) and 3(*h*)–(*j*). The difference method (*c*, *h*) does not solve the problem since it produces a lot of false alarms resulting from permanent structure motion and distortion. The partitioning scheme using Fourier analysis developed by Myagotin *et al.* (2009) already performs better, see plots (*d*, *i*), but still contains some artefacts. The approach discussed here can be seen to distinguish pore collapses from displacement in a more reliable manner, see plots (*e*, *j*).

5.2. Metal foams

The general application of metal foams is the fabrication of light-weight energy-absorbing components (Banhart, 2001). The components can be produced by a powder-metallurgical manufacturing route as follows. A compacted precursor material containing a metal powder and blowing agent are placed into the (shape-defining) mold that is afterwards heated in a furnace. Under heat treatment the material starts to foam *via* gas release from the blowing agent (Stanzick *et al.*, 2002) and eventually fills the foaming mold completely. Important requirements for the industrial components are homogeneous space-filling, high regularity of the cellular structure, and a rigid connection between the foam and the component's faces. An *in situ* coalescence analysis of the in-mold foaming allows one to assess the evolution of the foam concerning the above requirements.

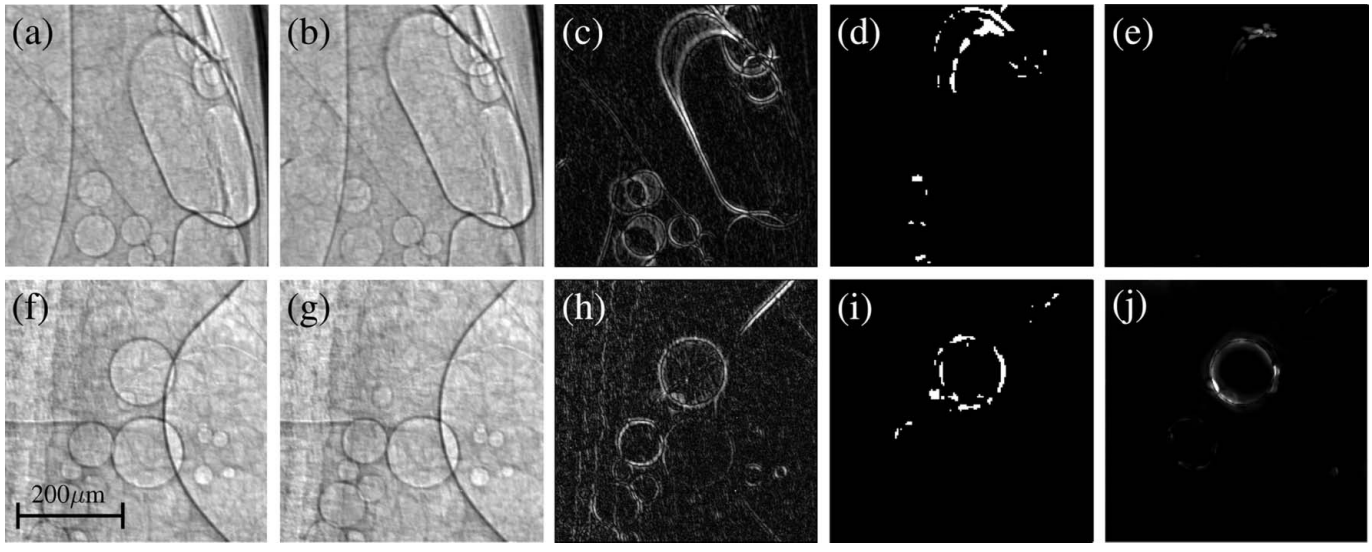

Figure 3
Detection of single coalescence events in aqueous foam: original successive radiographs (*a*, *b*) and (*f*, *g*) for two foaming durations; (*c*, *h*) difference images between the two successive frames; (*d*, *i*) coalescence maps produced by the Fourier shift detection; (*e*, *j*) coalescence maps produced by the method presented here. Both difference images (*c*, *h*) contain strong motion-related artefacts, which are also partly present in (*d*, *i*), while the map (*j*) reflects well the underlying bubble collapse.

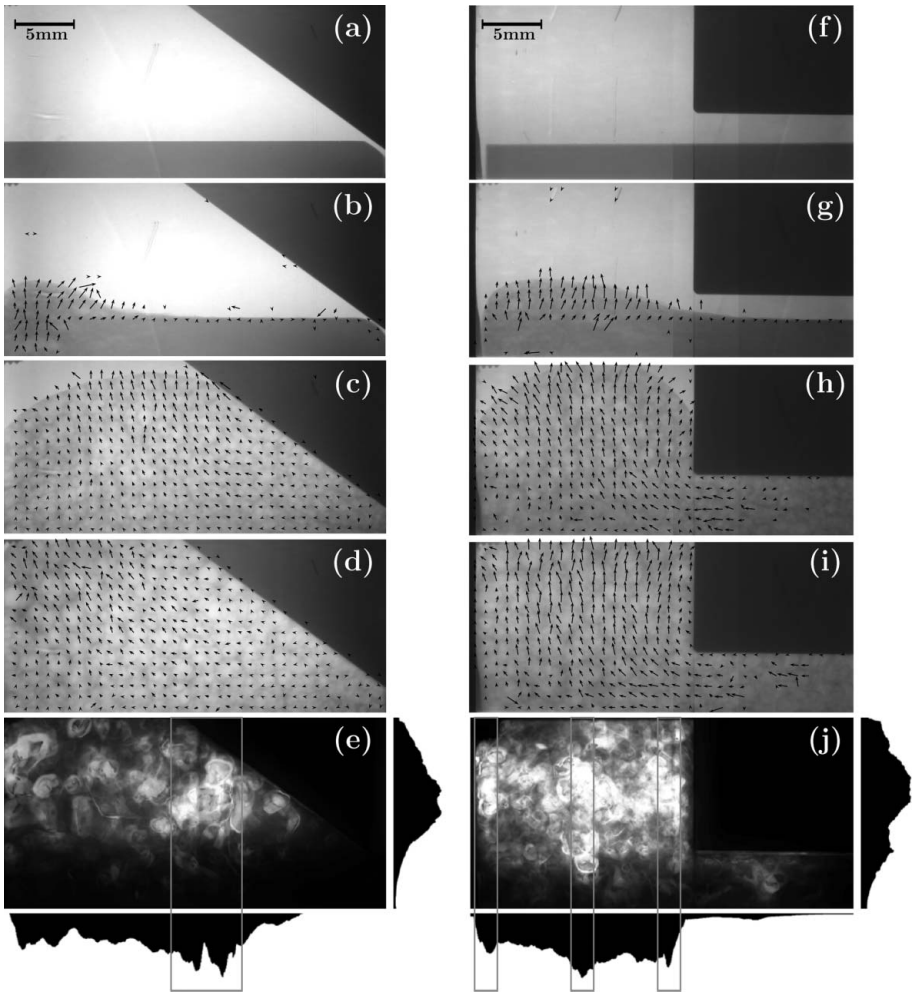

Figure 4
Estimated velocity fields for two metal foaming samples at different expansion stages: (left) foaming in a wedge-shaped mold at (*a*) 0 s, (*b*) 20 s, (*c*) 45 s and (*d*) 65 s; (right) foaming in an L-shaped mold at (*f*) 0 s, (*g*) 25 s, (*h*) 50 s, (*i*) 60 s. Plots (*e*) and (*j*) show integral coalescence distributions. The vertical coalescence event profiles reveal a lower events fraction in the bottom foam layers, where film thinning is slowed down by a liquid material flow from upper layers. The non-uniform horizontal event distributions can be explained by frictional forces between the upward-moving foam flows and steel molds.

In the following experiment two baking cups made from steel were prepared. Wedge-shaped and L-shaped molds were selected, each 10 mm in depth. As a temporal origin we chose the moment at which the samples start to foam. Fig. 4 illustrates both foaming processes and estimated velocity vector fields. At the beginning the samples expand mostly on the left-hand side producing bumps of semi-liquid material. This is caused by a non-uniform heating within the molds. With the course of time the right-hand foam front overtakes that on the left-hand side. In the final expansion stage we observe a slow continuous flow of the foamed material oriented parallel to the inclined border in the wedge-shaped mold (*d*) and along the cavity to the left and upwards in the L-shaped one (*i*).

For both samples we constructed integral coalescence maps. The corresponding plots are demonstrated in Figs. 4(*e*) and 4(*j*). Additionally, the horizontal and vertical integral coalescence distributions are plotted. A vertical event distribution reflects a small number of collapses on the bottom and a high fraction of events in the middle of the samples, as expected. The downward liquid flows (induced mostly by gravitational forces) supply the bottom layers of the foam with liquid melt. This delays the thinning of the bottom foam films, and produces the vertical gradient of coalescence events. The estimated data are well in accordance with data estimated earlier (Babcsán *et al.*, 2007).

The horizontal plots reveal an anomalous effect, however. One recognizes a high fraction of coalescence events on the right-hand side of the wedge-shaped sample (*e*); in the plot (*j*) we observe an increased fraction of coalescence events in the middle and on the left- and right-hand sides of the mold. The corresponding image regions are highlighted by the grey rectangles. The first interpretation of this effect could be a low foam stability resulting from significant friction forces between the upward moving foam front and the steel mold. Friction forces promote film stretching and additional topological rearrangements of the foam films which destabilize the foam structure, especially at the mold's faces. The importance of this observation is that already during the manufacturing stage of lightweight components one can predict the locations of possible detachments of the metal foam from the requested profile.

5.3. Polymer foams

A common receipt for generating stable foams is the inclusion of solid particles in the liquid phase. The particles are thought to increase the viscosity of the liquid and thus stabilize cell walls (Verdejo *et al.*, 2009). In this section we analyze this technique quantitatively comparing unfilled and filled silicone polymer foams. The polymer matrix was an unfilled polydimethylsiloxane (PDMS) foam supplied by Bluestar Silicones (Rhodorsil RTFoam 3240) as a two-part system. PDMS foams are obtained from the reaction between a silanol (SiOH) on the hydroxyl-terminated polydimethylsiloxane reactant and a silane (SiH) on the polymethylhydrogensilane reactant in the presence of Pt catalyst and with the evolution of hydrogen. Foaming takes place at room temperature as an exothermic reaction. Aligned multi-walled carbon nanotubes (MWNT) were synthesized in-house by a chemical vapour deposition (CVD) technique. The MWNTs were dispersed by high shear mixing in the polymethylhydrogensilane reactant to avoid inhibiting the Pt

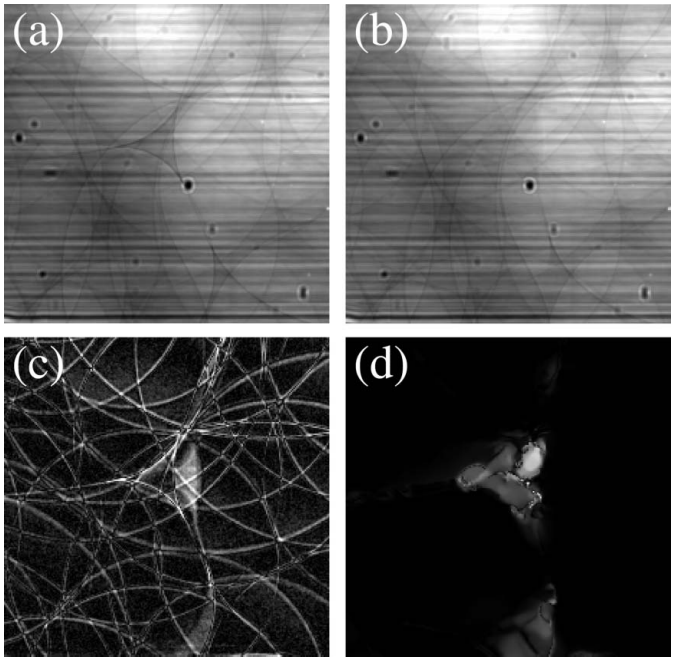

Figure 5
Imaging of a polymer foam sample (CONT): (a, b) sequential radiographic frames; (c) difference image; (d) coalescence map. The map renders well the disappeared Plateau border even in the presence of structural motion and static noise in the original radiographs.

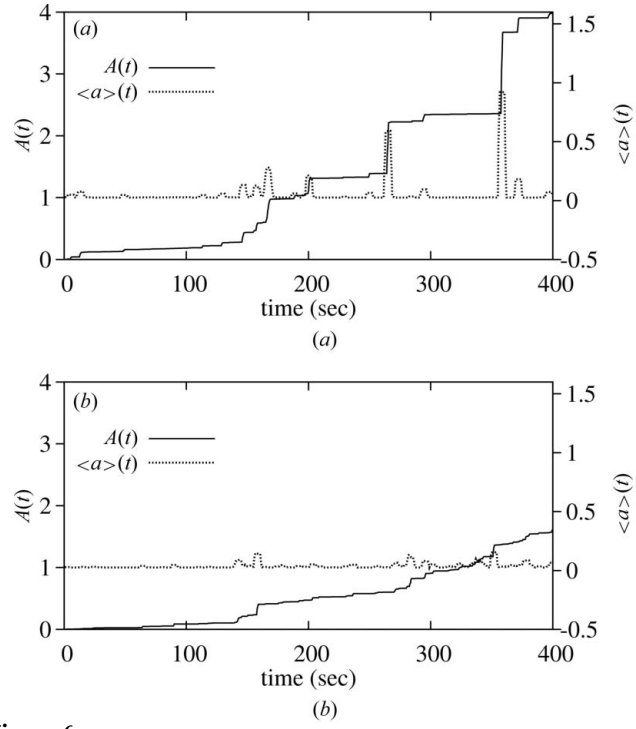

Figure 6
Coalescence rates for (a) CONT and (b) CVD samples (all characteristics are given in arbitrary units). A lower slope of the integral coalescence fraction $A(t)$ in the case of the CVD foam shows evidence of a higher stability of the foam filled with nanoparticles.

catalyst. The two compounds were finally mixed at a 1:1 ratio for 1 min while the safety protocol at ESRF was followed. In this section we consider two samples containing 0 and 0.2 wt% of MWNT, called hereafter CONT and CVD, respectively.

The internal structure of samples while foaming can be understood from the radiographic frames in Figs. 5(a) and 5(b). The images contain a pronounced intensity modulation introduced by multilayer monochromator optics (Rack *et al.*, 2010). In the middle of the difference plot in Fig. 5(c) one recognizes a typical coalescence event. The white fringes in the image appear owing to the slight shift of the foam constituents. A computed coalescence map for the frames is given in Fig. 5(d). Although the original images suffer from a strong statical background, the coalescence map renders the location of vanished material quite well.

In order to quantify the coalescence processes, a running average for the coalescence rate $\langle a\rangle(t)$ and integral coalescence fraction $A(t)$ are plotted for both samples in Fig. 6. The former corresponds to the number of pixels contained in the coalescence area determined. The latter is the total coalescence rate $\langle a\rangle(t)$ integrated over a time interval $[0, t]$. The formal definitions for the characteristics are given by Myagotin *et al.* (2009).

For both samples, already soon after the onset of the foaming the first coalescence events are detected which are reflected by peaks in the coalescence rate $\langle a\rangle(t)$. The events have a low amplitude corresponding to a small radiographic projection area. With the course of time the two chosen samples evolve quite differently. It becomes evident that in the case of CONT foam there exist relatively sparse events with rather high amplitude which indicates large coalescing bubbles.

The integral coalescence of the CVD sample, in contrast, is a more continuous function exhibiting an almost constant number of low-intensity film ruptures per unit time. On comparing the two samples we notice that the CONT foam exhibits a significantly higher integral coalescence than CVD. These observations support the hypothesis that, owing to an increased viscosity of the liquid or decoration of the cell walls by the nanoparticles, capillary drainage in the filled sample is significantly reduced. This in turn leads to a reduced film thinning rate and to more stable liquid films separating the bubbles, and consequently to more stable foams.

6. Conclusion

The systematic use of radiography combined with optical flow computations allows one to analyze coalescence processes for a diversity of materials. By introducing the concept of a forward–backward check we were able to increase detection reliability and improve quantification of coalescence.

The presented approach is suitable for the detection and localization of individual film or bubble collapses as well as for the estimation of spatial and temporal distributions of the coalescence events.

The method is applicable to foams of different types provided that they can be monitored by an appropriate (*e.g.* X-ray) projection technique. Furthermore, the original resolution of the images in the projection sequence is preserved

and the results are of continuous nature (*i.e.* not computed in a binarized form).

Finally, we would like to point out that the methods developed are not restricted to the problem of coalescence detection in evolving foams or emulsions. Different sudden processes such as fast rearrangement in a uniform motion pattern for particle flow in thixo- or rheocasting processes (Zabler *et al.*, 2010) could also be addressed in this manner.

The authors acknowledge the European Synchrotron Radiation Facility (Grenoble, France) for beam time and wish to thank V. Gergely (University of Cambridge, UK) and J. Banhart (Helmholtz-Centre Berlin, Germany) for kindly providing the precursor materials for metal foam generation, and H. Stanzick, J. Moosmann, D. Hänschke, M. Mar Bernal and N. Bitinis for support during the foaming experiments.

References

Alvarez, L., Deriche, R., Papadopoulo, T. & Sánchez, J. (2007). *Int. J. Comput. Vis.* **75**, 371–385.
Babcsán, N., García-Moreno, F. & Banhart, J. (2007). *Colloids Surf. A*, **309**, 254–263.
Babin, P., Valle, G. D., Chiron, H., Cloetens, P., Hoszowska, J., Pernot, P., Réguerre, A. L., Salvo, L. & Dendievel, R. (2006). *J. Cereal Sci.* **43**, 393–397.
Baker, S., Scharstein, D., Lewis, J., Roth, S., Black, M. & Szeliski, R. (2011). *Int. J. Comput. Vis.* **92**, 1–31.
Banhart, J. (2001). *Prog. Mater. Sci.* **46**, 559–632.
Banhart, J., Stanzick, H., Helfen, L. & Baumbach, T. (2001*a*). *Appl. Phys. Lett.* **78**, 1152–1154.
Banhart, J., Stanzick, H., Helfen, L., Baumbach, T. & Nijhof, K. (2001*b*). *Adv. Eng. Mater.* **3**, 407.
Belaroui, F., Cabane, B., Dorget, M., Grohens, Y., Marie, P. & Holl, Y. (2003). *J. Colloid Interface Sci.* **262**, 409–417.
Bhakta, A. & Ruckenstein, E. (1997). *J. Colloid Interface Sci.* **191**, 184–201.
Biance, A.-L., Cohen-Addad, S. & Höhler, R. (2009). *Soft Matter*, **5**, 4672–4679.
Brox, T., Bruhn, A., Papenberg, N. & Weickert, J. (2004). *Computer Vision–ECCV 2004*, *Lecture Notes in Computer Science*, Vol. 3024, edited by T. Pajdla and J. Matas, pp. 25–36. Berlin: Springer.
Bruhn, A. & Weickert, J. (2005). *Proceedings of the Tenth IEEE International Conference on Computer Vision*, Vol. 1, pp. 749–755.
Carrier, V. & Colin, A. (2003). *Langmuir*, **19**, 4535–4538.
Dale, C., West, C., Eade, J., Rito-Palamares, M. & Lyddiatt, A. (1999). *Chem. Eng. J.* **72**, 83–89.
Dubsky, S., Jamison, R. A., Irvine, S. C., Siu, K. K. W., Hourigan, K. & Fouras, A. (2010). *Appl. Phys. Lett.* **96**, 023702.
Durand, M. & Stone, H. A. (2006). *Phys. Rev. Lett.* **97**, 226101.
Dzieciol, K., Isaac, A., Sket, F., Borbély, A. & Pyzalla, A. R. (2009). *TMS Annual Meeting*, pp. 15–22.
García-Moreno, F., Fromme, M. & Banhart, J. (2003). *Cellular Metals and Metal Foaming Technology*, edited by J. Banhart, N. Fleck and A. Mortensen, pp. 89–94. Bremen: Verlag-MIT.
García-Moreno, F., Rack, A., Helfen, L., Baumbach, T., Zabler, S., Babcsán, N., Banhart, J., Martin, T., Ponchut, C. & Di Michiel, M. (2008). *Appl. Phys. Lett.* **92**, 134104.
Gergely, V. & Clyne, T. (2004). *Acta Mater.* **52**, 3047–3058.
Gruner, S., Tate, M. & Eikenberry, E. (2002). *Rev. Sci. Instrum.* **73**, 2815–2842.
Helfen, L., Baumbach, T., Cloetens, P., Stanzick, H., Schladitz, K. & Banhart, J. (2005). *Appl. Phys. Lett.* **86**, 231907.
Helfen, L., Baumbach, T., Stanzick, H., Banhart, J., Elmoutaouakkil, A. & Cloetens, P. (2002). *Adv. Eng. Mater.* **4**, 808–813.
Helfen, L., Stanzick, H., Ohser, J., Schladitz, K., Pernot, P., Banhart, J. & Baumbach, T. (2003). *Proc. SPIE*, **5045**, 254–265.
Horn, B. & Schunck, B. (1981). *Artif. Intell.* **17**, 185–203.
Ireland, P. M. (2009). *Chem. Eng. Sci.* **64**, 4866–4874.
Lambert, J., Cantat, I., Delannay, R., Mokso, R., Cloetens, P., Glazier, J. A. & Graner, F. (2007). *Phys. Rev. Lett.* **99**, 058304.
Lambert, J., Mokso, R., Cantat, I., Cloetens, P., Glazier, J. A., Graner, F. & Delannay, R. (2010). *Phys. Rev. Lett.* **104**, 248304.
Maire, E. & Buffiere, J. (2000). In *X-ray Tomography in Material Science*, edited by J. Baruchel, J. Y. Buffiere, E. Maire, P. Merle and G. Peix, pp. 115–125. Paris: Hermes Science.
Metz, C. E. (1978). *Semin. Nucl. Med.* **8**, 283–298.
Middendorf, M. & Nagel, H.-H. (2001). In *Eighth IEEE International Conference on Computer Vision*, Vol. 1, pp. 178–183.
Müller, W. & di Meglio, J. (1999). *J. Phys. Condens. Matter*, **11**, L209–L215.
Myagotin, A., Helfen, L. & Baumbach, T. (2009). *Meas. Sci. Technol.* **20**, 055703.
Rack, A., García-Moreno, F., Baumbach, T. & Banhart, J. (2009*a*). *J. Synchrotron Rad.* **16**, 432–434.
Rack, A., Helwig, H.-M., Bütow, A., Rueda, A., Matijasevic-Lux, B., Helfen, L., Goebbels, J. & Banhart, J. (2009*b*). *Acta Mater.* **57**, 4809–4821.
Rack, A., Weitkamp, T., Riotte, M., Grigoriev, D., Rack, T., Helfen, L., Baumbach, T., Dietsch, R., Holz, T., Krämer, M., Siewert, F., Meduna, M., Cloetens, P. & Ziegler, E. (2010). *J. Synchrotron Rad.* **17**, 496–510.
Rouyer, F., Cohen-Added, S., Vignes-Adler, M. & Höhler, R. (2003). *Phys. Rev. E*, **67**, 021405.
Schüth, F., Sing, K. S. W. & Weitkamp, J. (2002). Editors. *Handbook of Porous Solids*. Weinheim: Wiley-VCH.
Søndergaard, K. & Lyngaae-Jørgensen, J. (1996). *Polymer*, **37**, 509–517.
Stanzick, H., Wichmann, M., Weise, J., Helfen, L., Baumbach, T. & Banhart, J. (2002). *Adv. Eng. Mater.* **4**, 814–823.
Swets, J. A. (1988). *Science*, **240**, 1285–1293.
Swets, J. A., Dawes, R. M. & Monahan, J. (2000). *Sci. Am.* **283**, 82–87.
Vandewalle, N., Lentz, J. F., Dorbolo, S. & Brisbois, F. (2001). *Phys. Rev. Lett.* **86**, 179–182.
Verdejo, R., Tapiador, F. J., Helfen, L., Bernal, M. M., Bitinis, N. & Lopez-Manchado, M. A. (2009). *Phys. Chem. Chem. Phys.* **11**, 10860–10866.
Weaire, D. & Hutzler, S. (1999). *The Physics of Foams.* Oxford: Clarendon.
Weitkamp, T., Tafforeau, P., Boller, E., Cloetens, P., Valade, J.-P., Bernard, P., Peyrin, F., Ludwig, W., Helfen, L. & Baruchel, J. (2010). *AIP Conf. Proc.* **1234**, 83–86.
Wickens, T. (2001). *Elementary Signal Detection Theory*. Oxford University Press.
Wübben, T., Stanzick, H., Banhart, J. & Odenbach, S. (2003). *J. Phys. Condens. Matter*, **15**, 427–433.
Zabler, S., Rack, A., Rueda, A., Helfen, L., Garcia-Moreno, F. & Banhart, J. (2010). *Phys. Status Solidi A*, **207**, 718–723.
Zimmer, H., Bruhn, A. & Weickert, J. (2011). *Int. J. Comput. Vis.* **93**, 368–388.